Supporting Information for

Self-healing of electrical damage in insulating robust epoxy containing dynamic fluorine-substituted carbamate bonds for green dielectrics

*Wenjie Sun, Jiazhu Xu, Jianhong Song, Yue Chen, Zepeng Lv, Yonghong Cheng, Lei Zhang**

State Key Laboratory of Electrical Insulation and Power Equipment, School of Electrical Engineering, Xi'an Jiaotong University, Xi'an 710049, PR China

*Corresponding Author *E*-mail: lzhangac@xjtu.edu.cn

● Experimental section

Materials

Bisphenol-A epoxy resin (EP, epoxy value: 0.51 eq./100 g) was obtained from Shandong Usolf Chemical Technology, China. 1,4-Butylene glycol (BDO) and 2,2,3,3-tetrafluoro-1,4-butanediol (4FBDO) were obtained from Energy Chemical, China. Dichloromethane (CH_2Cl_2), hexamethylene diisocyanate (HDI) and ethylene glycol (EG) were supplied from Meryer Chemical Technology, China. N, N-Dimethylbenzylamine (BDMA) and Dibutyltin dilaurate (DBTDL) were provided by Macklin, China. Methyltetrahydrophthalic anhydride (MTHPA) was obtained from Aladdin, China. All these chemicals were directly used as received.

Preparation of hydroxy-terminated epoxy

2 mmol of Diols (BDO or 4FBDO), 1 mmol of EP, and two drops of BDMA were mixed in a beaker equipped with a magnetic stirrer at 100 ℃ for 3h [1]. According to our

previous study, the best healability can be achieved when the stoichiometric ratio of diols and epoxy ring groups is two [2]. The prepared linear polymers were named EP-BDO and EP-4FBDO, respectively.

Preparation of epoxy containing dynamic fluorinated carbamate bonds

5.54 g of EP-4FBDO was dissolved in CH_2Cl_2 in a beaker. 3.52 g of HDI and two drops of DBTDL were then introduced to build the healable and cross-linked epoxy. EP-FCB was obtained through solution-casting and dried in an oven at 90 ℃ for 6 h. As a comparison, epoxy without fluorine substitution (EP-CB) was prepared in the same way, except using EP-BDO to replace EP-4FBDO.

General characterization information

Fourier Transform Infrared (FTIR) spectra were carried out using a spectrometer (IN10+IZ10, America) ranging from 400–4000 cm^{-1} at room temperature. ^1H Nuclear Magnetic Resonance (NMR) spectra were recorded using a spectrometer (JNM-ECZ400S/L1, Japan) with a frequency of 400 MHz. Temperature-dependent FTIR was performed on a spectrometer (Bruker INVENIO X) ranging from 500–4000 cm^{-1} from 30 ℃ to 180 ℃.

Dynamic mechanical analysis (DMA) was conducted on an instrument (Netzsch DMA242E) in a tension film mode. Rectangular samples were tested at a frequency of 1 Hz and a strain of 0.1 %. A heating rate of 3 ℃·min^{-1} was applied from room temperature to 150 ℃. The glass transition temperature (T_g) is the peak point of tanδ.

Stress-strain curves were measured using a universal testing machine (CMT4503-5kN) at room temperature with a tensile speed of 2 mm·min^{-1}. Rectangular specimens were

prepared with 80 × 5 × 0.5 mm.

The rheological properties test was experimented on a rheometer (Anton Paar MCR302). A temperature swept from room temperature to 180 ℃ was performed with a heating rate of 3 ℃/min at a frequency of 1 Hz.

The volume resistance at room temperature of the samples of ca. 0.5 mm was measured by 6517B with a three-electrode system.

Thermally stimulated current (TSC) tests were performed on a Novocontrol Concept 90 system. The samples were first heated to 5 ℃ above T_g and polarized with an electrical field of 2 MV/m for 30 min, followed by quickly cooling to -100 ℃. Tests were carried out by rising the temperature from -100 ℃ to 180 ℃ with a heating rate of 5 ℃/min in a nitrogen atmosphere.

AC and DC breakdown strength tests were carried out on a computer-controlled breakdown instrument (GJW-100kV, Changchun, China) with a plate-plate electrode system. The electrodes and the samples with a thickness of ca. 0.2 mm were immersed in silicone oil to avoid surface flashover. The voltage was increased with a rate of 2 $kV \cdot s^{-1}$ until the sample got a breakdown. Breakdown strength was evaluated by the Weibull analysis according to Equation (S1).

$$P(E) = 1 - \exp\left[-\left(\frac{E}{E_0} \right)^{\beta} \right] \quad \text{(S1)}$$

whereby P is the failure probability, E is the measured electrical breakdown strength, E_0 is the scale parameter, and the β is the shape parameter. In total, ten samples for each type of material were tested for Weibull analysis.

Permittivity and loss factor (Tan δ) were determined using a dielectric analyzer

(Technologies Concept 80) with frequency ranging from 10^{-1} to 10^{6} Hz at room temperature. The thickness of the sample is about 1 mm, and gold electrodes with a diameter of 30 mm were sprayed on the surface of the samples for the test.

Swelling tests

The experiment was conducted by immersing the specimens in CH_2Cl_2 for 24h before evaluating the swelling ratio, according to Equation (S2). After that, the insoluble materials were dried in a vacuum drying oven until the weight reached a constant, and the gel fraction was obtained according to Equation (S3).

$$\text{swelling ratio} = \frac{(m_1 - m_0)}{m_0} \times 100\% \quad \text{(S2)}$$

$$\text{gel fraction} = \frac{m_2}{m_0} \times 100\% \quad \text{(S3)}$$

where m_0 is the original weight of the sample, m_1 is the mass of the sample after swelling, and m_2 is the mass of the sample after drying.

Reprocessing performance experiments

The samples were ground into powder, followed by hot-pressing under 20 MPa at different temperatures for 30 min. Reprocessability was evaluated based on mechanical and insulating performance. Reprocessing efficiency (γ) was calculated as the ratio of the property recovery ratio of the recycled specimens ($P_{\text{reprocessed}}$) to the original specimen (P_{original}).

$$\gamma = \frac{P_{\text{reprocessed}}}{P_{\text{original}}} \times 100\% \quad \text{(S4)}$$

where P can be tensile stress, tensile strain, volume resistivity, and breakdown strength.

Cut-healing experiments

The rectangular film was cut into two parts by a clean blade, and then the separated sample pieces were closely placed, followed by heating at different temperatures. The changes in the sample features were observed through a polarizing microscope (BX51–P). The healing efficiency (η) was calculated as the ratio of the tensile stress and strain of the healed specimen (P_{healed}) to the original specimen (P_{original}).

$$\eta = \frac{P_{\text{healed}}}{P_{\text{original}}} \times 100\% \quad \text{(S5)}$$

Electrical treeing and healing experiments

The experiments were carried out by using a typical needle-plate electrode configuration, whereby the steel needle electrode with a tip radius of 25±5 μm is embedded in the sample to simulate the electrical defect. The insulation distance between the needle tip and the plate electrode is ac. 2.0 mm. A measurement system consisting of a power module, an optical observation module and a partial discharge module. The prepared samples were immersed in silicone oil to avoid surface discharges, and AC voltage (50 Hz) with an amplitude of 15 kV (the tree inception voltage is 14.39 kV) was applied to the samples for 15 min at room temperature. The morphologies of electrical trees in epoxy were recorded. And the apparent discharge magnitude was also tested by the OMICRON MPD600 instrument. The damaged samples were healed at 180 ℃/15 MPa for 30 min. The chemical structure around the electrical tree channel was tested by Micro-infrared spectroscopy (Bruker VERTEX70).

Degradation performance experiments

The cured epoxies and composites were immersed in EG solution at 180 ℃. The degradation rate (v_d) is calculated as the following equation：

$$v_d = \frac{(m_0 - m_r)}{t_d \cdot V} \times 100\% \quad \text{(S6)}$$

where m_0 is the original weight of the sample, m_r is the mass of residual sample after being washed with deionized water and drying, t_d is the degradation time and V is the EG volume.

- **Chemical structure characterization of epoxy without fluorine atoms:**

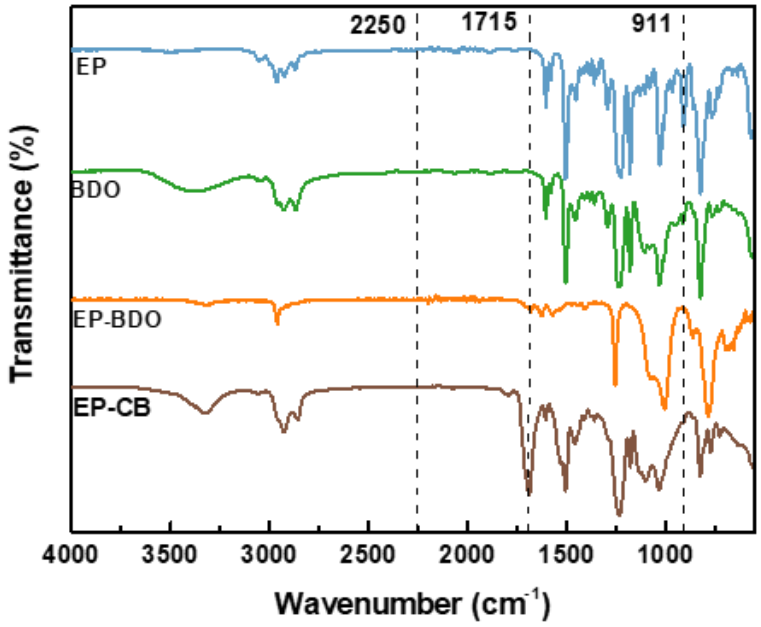

Fig. S1. FTIR spectra of EP, BDO, EP-BDO and EP-CB.

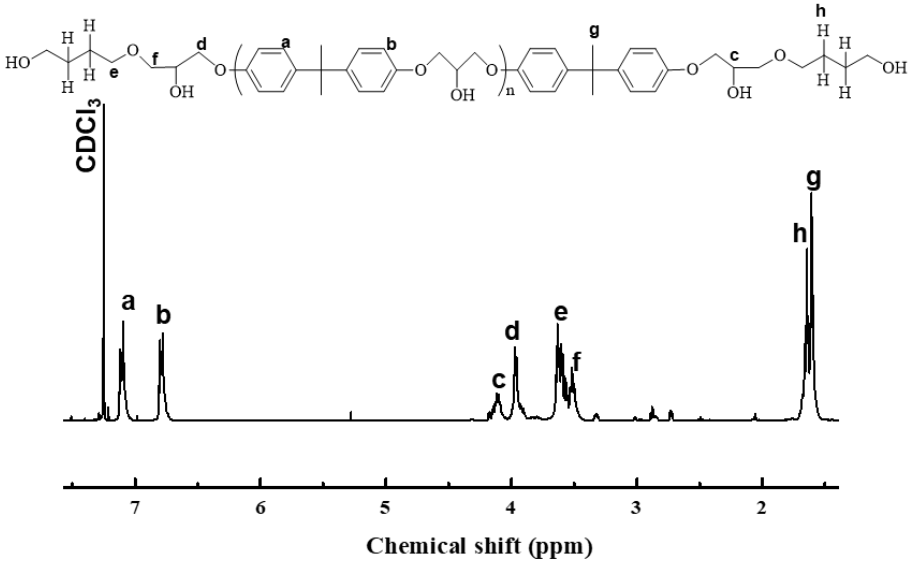

Fig. S2. ^{1}H NMR curve of EP-BDO.

- **Swelling experiments:**

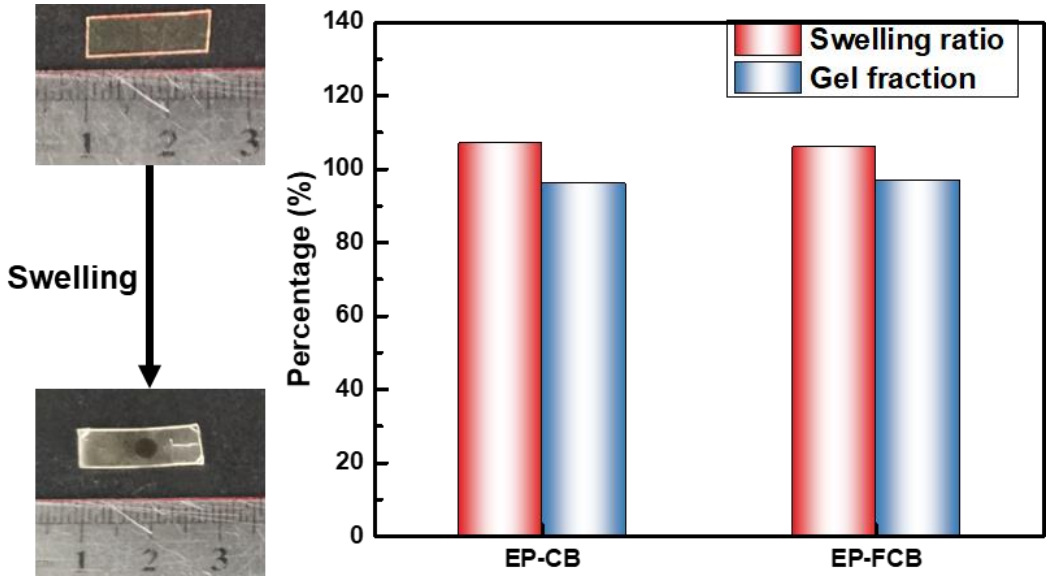

Fig. S3. Swelling ratio and gel fraction of EP-CB and EP-FCB.

- **Thermal performance:**

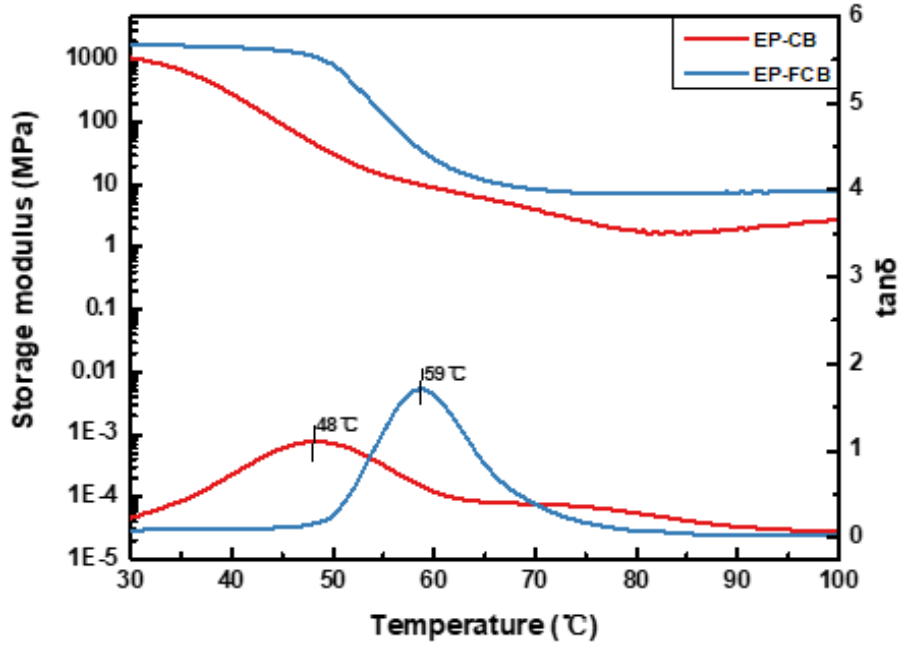

Fig. S4. DMA curves of EP-CB and EP-FCB. The T_gs of EP-CB and EP-FCB are 48 ℃ and 59 ℃, respectively.

- **Mechanical properties:**

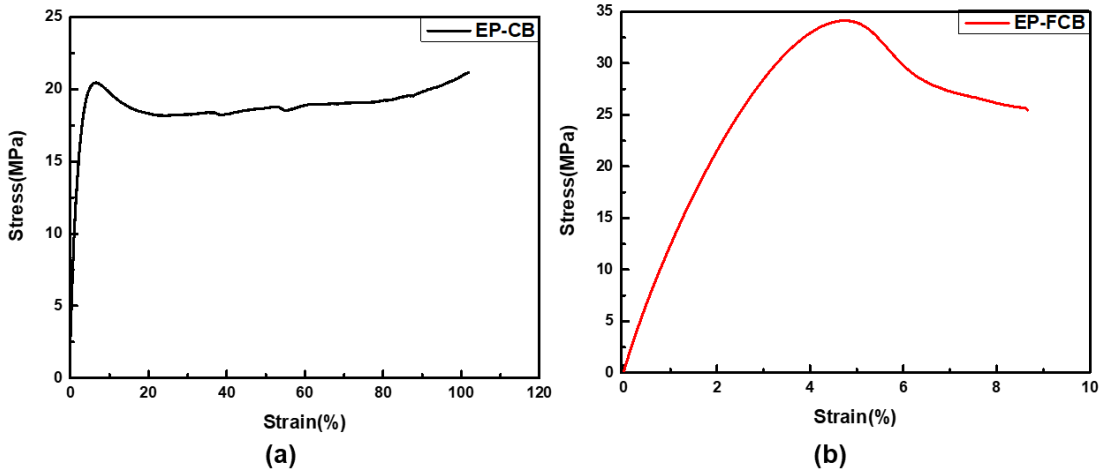

Fig. S5. Stress-strain curves of EP-CB and EP-FCB

Table S1. Mechanical properties of the prepared epoxy.

Samples	σ^a (MPa)	ε^b (%)	E^c (MPa)
EP-CB	21.1±0.2	98.6±4.7	571±15
EP-FCB	33.4±1.0	8.9±0.4	1217±33

[a]Tensile strength; [b]Elongation at break; [c]Elastic modulus.

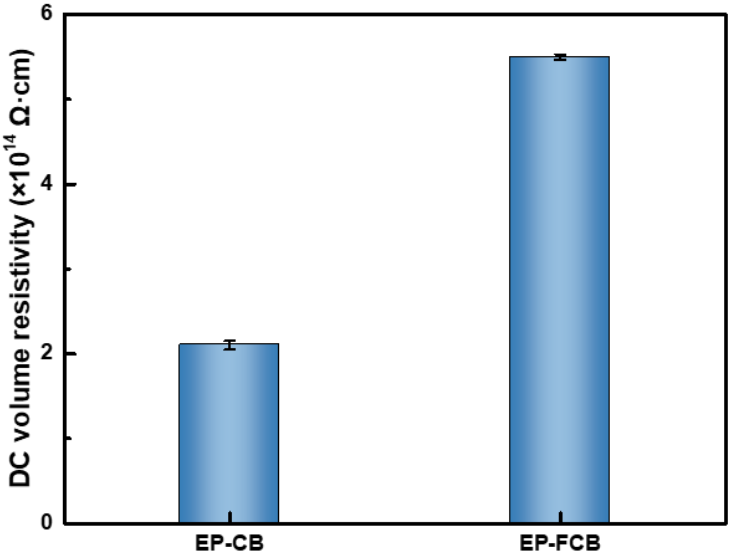

Fig. S6. The DC volume resistivity of EP-CB and EP-FCB.

- **TSC measurements:**

TSC curves is formed by the superposition of different current peaks. When peaks are unable to be directly distinguished when they are too close. Peak-fitting proves is performed to analysis the electrical properties of traps from TSC spectra. Table S2 concludes three fitted gaussian peaks.

Table S2. The calculated trap depth and trapped charge of each peak for EP-CB and EP-FCB.

Samples	T_{P1}[a] (℃)	H_{P1}[b] (eV)	Q_{P1}[c] (C/m^2)	T_{P2}[d] (℃)	H_{P2}[e] (eV)	Q_{P2}[f] (C/m^2)
EP-CB	82	0.78	0.026	104	1.33	0.063
EP-FCB	90	1.16	0.407	144	1.19	0.316

[a]The temperature of the P1 center; [b]The trap depth of peak P1; [c]The amount of trapped charge in P1; [d]The temperature of the P2 center; [e]The trap depth of peak P2; [f]The amount of trapped charge in P2.

- **Computational methods:**

To examine the influence of the fluorine atoms on the properties of carbamate bonds, two kinds of molecular structures (CB and FCB) were chosen for quantum chemical calculation, as shown in Fig. S7. The calculation was carried out with the Gaussian 16 program package. The 6-31 G basis function and B3LYP hybrid function by density functional theory (DFT) method are applied to calculate the highest occupied orbitals (HOMO), lowest unoccupied orbitals (LUMO) level, and electrostatic potential.

(a) (b)

Fig. S7. Theoretical modeling molecular structures. (a) CB, (b) FCB.

- **Dielectric performance:**

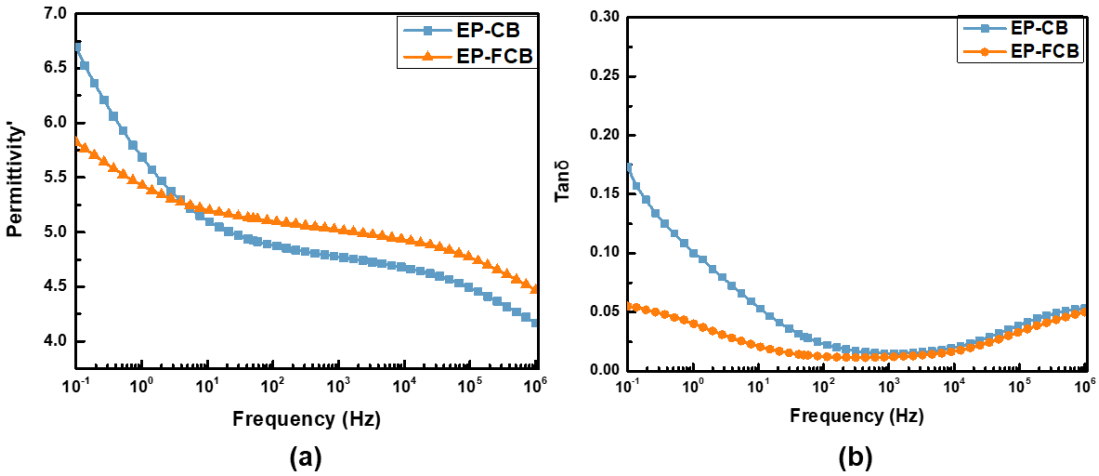

Fig. S8. Frequency-dependent changes of dielectric constant and loss.

- **Temperature-dependent FTIR spectra of EP-CB:**

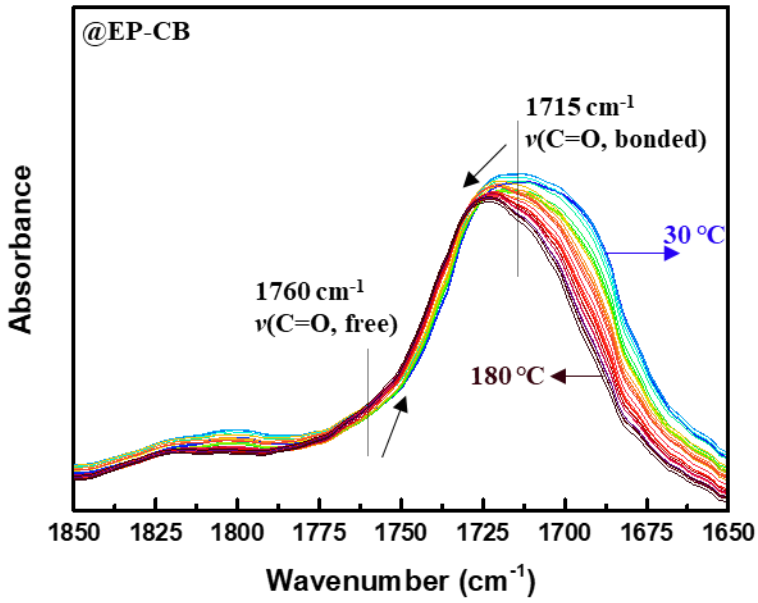

Fig. S9. Temperature-dependent FTIR spectra of EP-CB from 30 ℃ to 180 ℃, 1850−1650 cm^{-1}.

- **Stress relaxation curves:**

Stress relaxation analysis (SRA) was also performed on a Netzsch DMA242E DMA instrument utilizing rectangular films. The SRA experiments were performed in a strain control (2% strain) mode at a specified temperature. After equilibrating at this temperature for approximately 10 min, the stress decay was monitored. The relaxation modulus (G) was normalized by initial value (G_0). The characteristic relaxation time (τ) was defined as the time required for G/G_0 = 1/e with exponential decay function:

$$G(t) = G_0 e^{-t/\tau} \tag{S7}$$

The temperature dependence of the relaxation time of samples allows Arrhenius' law. According to the law, the activation energy (E_a) of various samples can be calculated using Equation (S8).

$$\ln(\tau) = \ln(\tau_0) + E_a / RT \tag{S8}$$

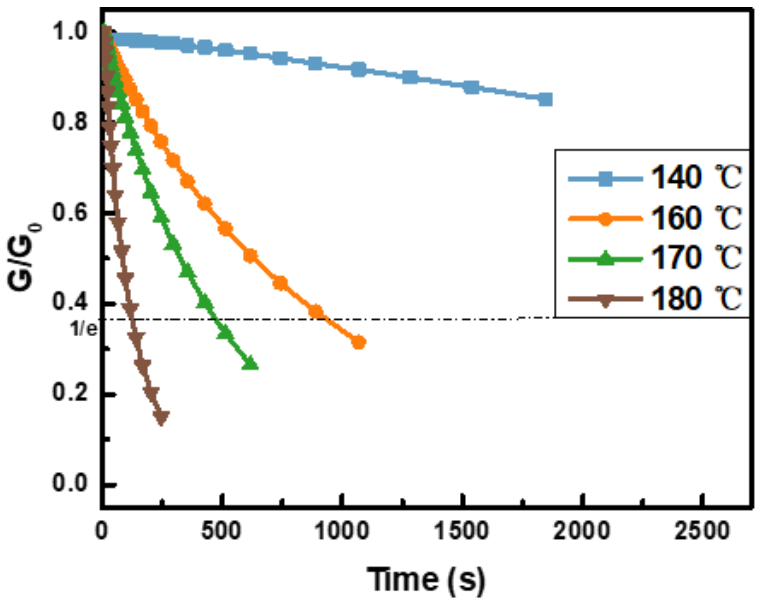

Fig. S10. Stress relaxation curves of EP-CB at different temperatures.

- **Rheological performance:**

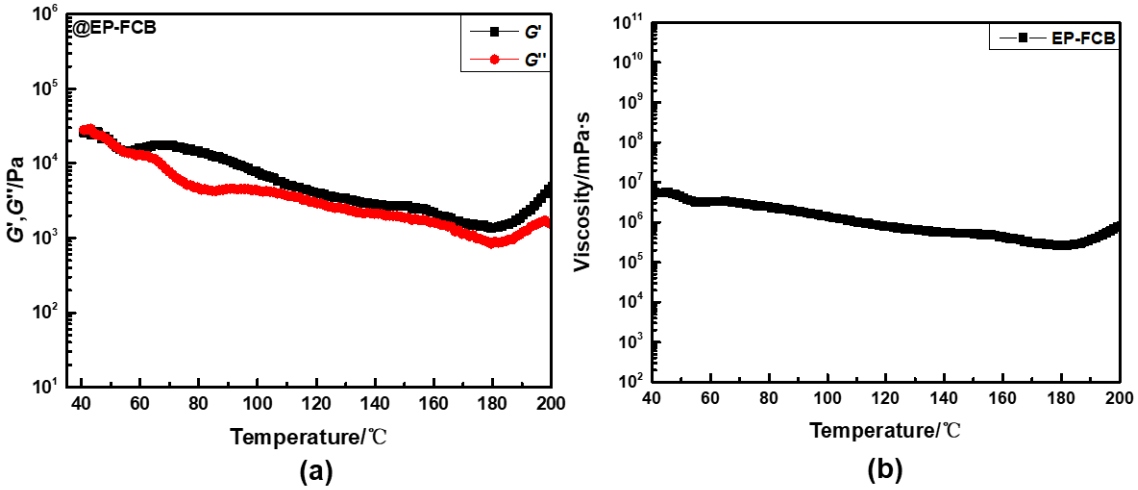

Fig. S11. Temperature sweep experiments of EP-FCB sample from the rheological analysis. (a) The storage modulus (*G*') and loss modulus (*G*'') curves, (b) viscosity.

- **Reprocessing ability:**

EP-CB and EP-FCB powders were hot-pressed at 140℃, 160℃, and 180℃. Fig. S11 demonstrates the photos of different epoxy after re-processing. Fig. S12 and Table S3 give the mechanical properties of samples after multiple reprocessing at 180 ℃/20 MPa. Fig. S13 and Fig. S14 exhibit the insulating properties of EP-CB after multiple reprocessing at 180 ℃/20 MPa.

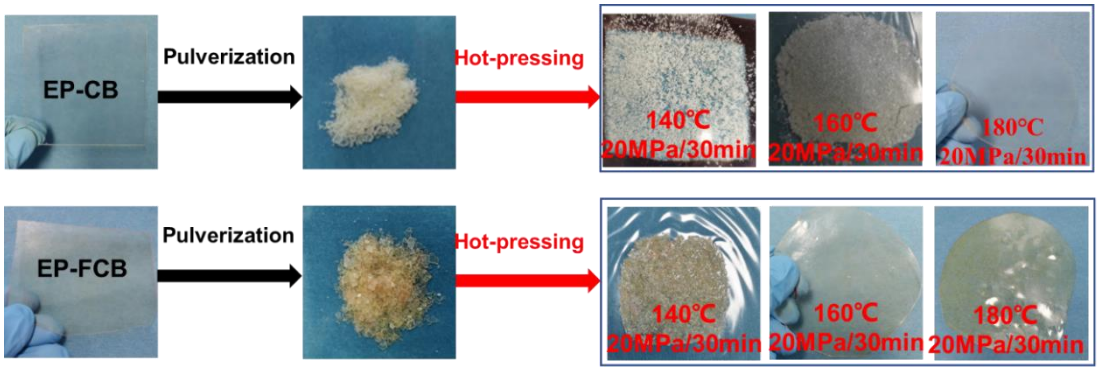

Fig. S12. Reprocessing ability of EP-CB and EP-FCB at different temperatures.

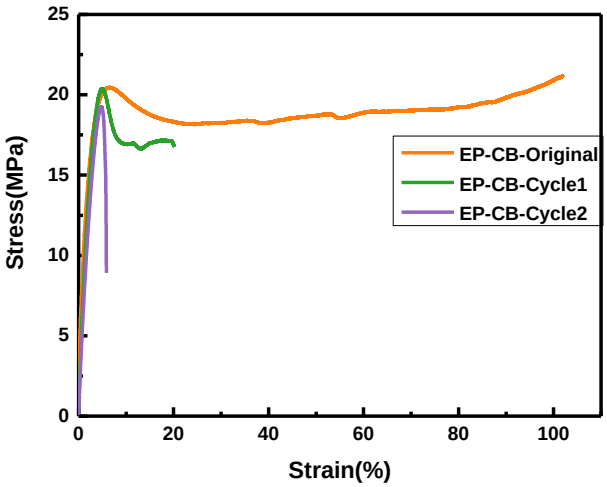

Fig. S13. Stress-strain curves of EP-CB after two cycles of reprocessing.

Table S3. Mechanical properties of the prepared epoxy after two cycles of reprocessing and the reprocessing efficiency.

Samples	Cycle1					
	σ^a (MPa)	ε^b (%)	E^c (MPa)	γ_σ (%)	γ_ε (%)	γ_E (%)
EP-CB	19.7±1.5	15.3±4.2	545±35	93	16	95
EP-FCB	32.8±0.7	7.3±0.8	848±28	98	82	70
Samples	Cycle2					
	σ^a (MPa)	ε^b (%)	E^c (MPa)	γ_σ (%)	γ_ε (%)	γ_E (%)
EP-CB	19.6±0.5	6.2±0.5	534±20	93	6	94
EP-FCB	28.7±1.0	7.0±0.8	837±37	86	79	69

[a]Tensile strength; [b]Elongation at break; [c]Elastic modulus.

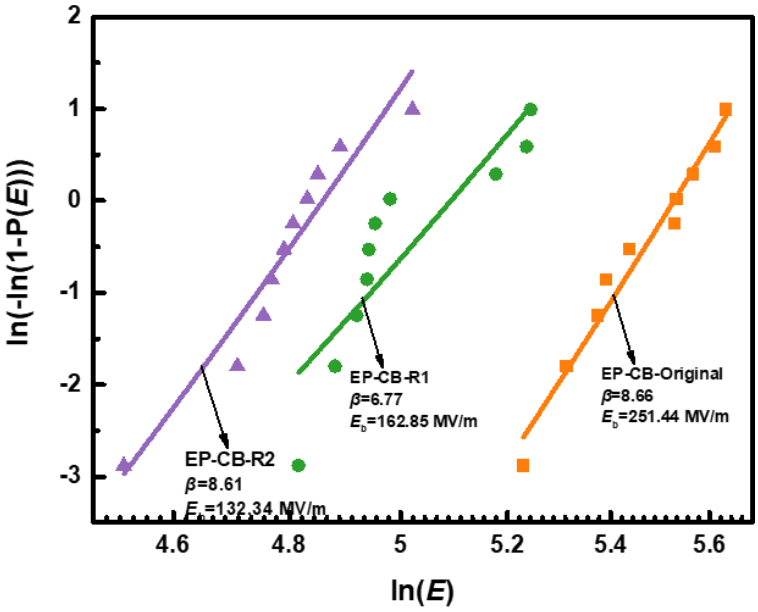

Fig. S14. Weibull plots of the breakdown strength of EP-CB after reprocessing.

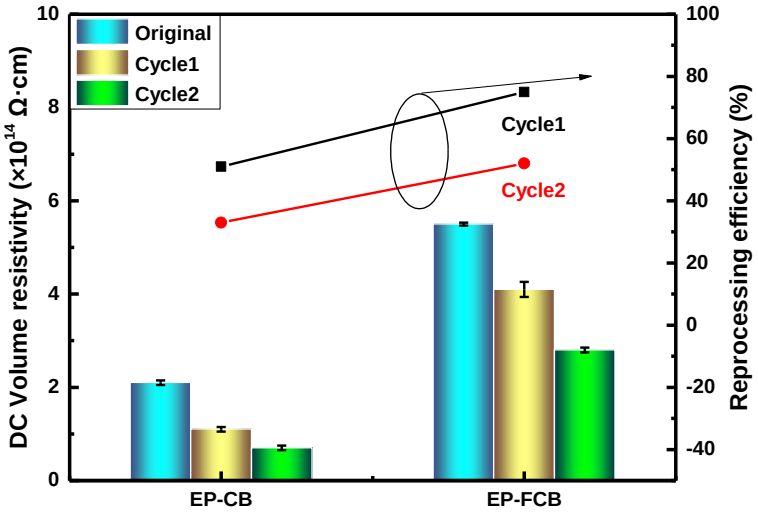

Fig. S15. DC volume resistivity and reprocessing efficiency based on volume resistivity.

- **Specimens for electrical tree:**

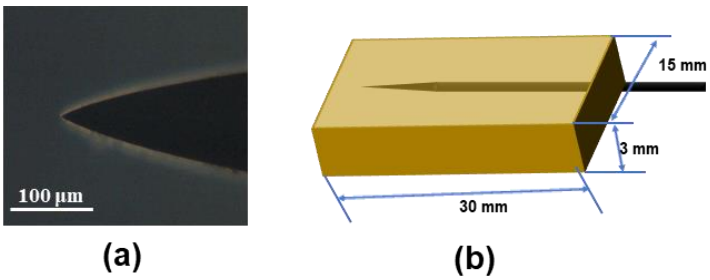

Fig. S16. (a) SEM image of the steel needle. (b) Schematic diagram of the sample for the electrical treeing experiments.

- **Testing of the tree inception voltage:**

Before the electrical treeing test, the tree initiation voltage was measured first. AC voltage (50 Hz) was applied to the prepared epoxy samples. The voltage was increased with a rate of 1 kV/10 min until the sample got an electric tree channel with the length of 10 mm. And the tree inception voltage was also evaluated by the Weibull analysis according to Equation (S9).

$$P(U) = 1 - \exp\left[-\left(\frac{U}{U_0}\right)^{\beta}\right] \quad \text{(S9)}$$

whereby P is the failure probability, U is the measured voltage, U_0 is the scale parameter, and the β is the shape parameter. In total, 10 samples for each type of material were tested for Weibull analysis.

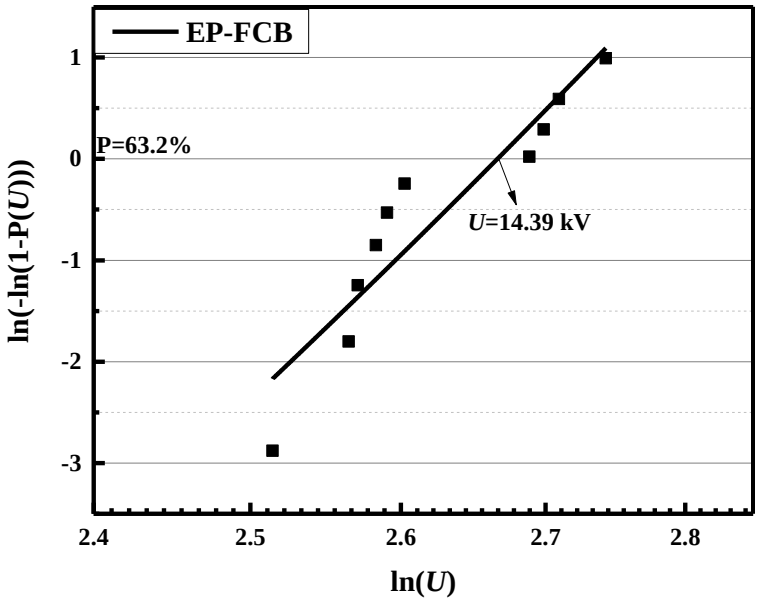

Fig. S17. Weibull plots of the tree inception voltage of EP-FCB.

- **Healing of electrical tree of EP-CB**

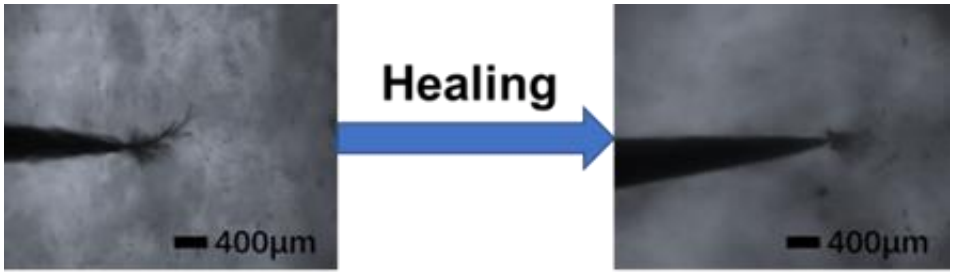

Fig. S18. The optical images of EP-CB before and after healing for electrical trees. After healing at180 ℃/15 MPa for 30 min, the electrical channels in EP-CB were partially healed as damage can be still observed.

- **Healing of electrical breakdown damage of EP-FCB slice samples:**

The electrical breakdown hole was produced through a plate-plate electrode system before healing at 180 ◦C/5 MPa for 30 min. The changes of the samples' micrographs were observed through a polarizing microscope (BX51–P). The healing efficiency was also calculated as the ratio of the breakdown strength of the healed specimen to the original specimen.

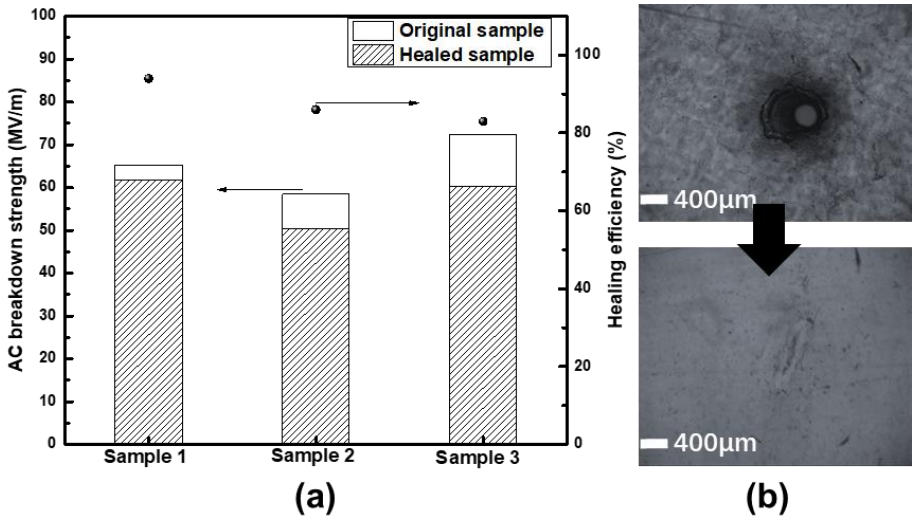

Fig. S19. (a) AC breakdown strength of the original EP-FCB and the healed EP-FCB. (b) Micrographs of EP-FCB before and after electrical breakdown-healing experiments.

- **Preparation of the normal epoxy resin cured by MTHPA**

EP was mixed with MTHPA with the weight ratio of 2:1 by magnetic stirring for 10 min. The mixture was degassed in a vacuum chamber at 60 ℃ for 30 min and then poured into a mould with the pre-inserted needle electrode to make the shape of epoxy resin meet the requirement of the test sample. The mixture was cured at 100 ℃ for 24 h to ensure the resin had been completely cured.

- **Breakdown voltage of EP-FCB before and after healing the electrical trees**

Table S4. The breakdown voltage of the original and the healed EP-FCB samples

Original sample	Breakdown voltage (kV)	Healed sample	Breakdown voltage (kV)
Sample 1	37.0	Sample 1	30.2
Sample 2	38.4	Sample 2	39.6
Sample 3	43.5	Sample 3	36.7
Average voltage	39.6±3.4	Average voltage	35.5±4.8

- **Preparation of EP-FCB based composites:**

The fresh glass fiber fabric was laid in the middle layer of the reactive EP-FCB and then cured under the same conditions of the preparation of EP-FCB. The morphology of glass fiber before and after recycling were obtained using a scanning electron microscope (SEM, GEMINI 500, ZEISS) at an acceleration voltage of 10 kV.

- **Soak the EP-FCB sample in EG solution at room temperature:**

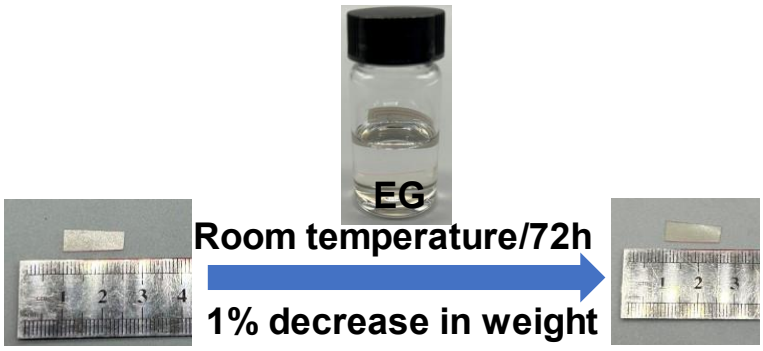

Fig. S20. Photos of EP-FCB sample soaked in EG solution at room temperature for 72 h. The weight of the sample is not significantly lost.

- **The protection of EP-FCB on the components:**

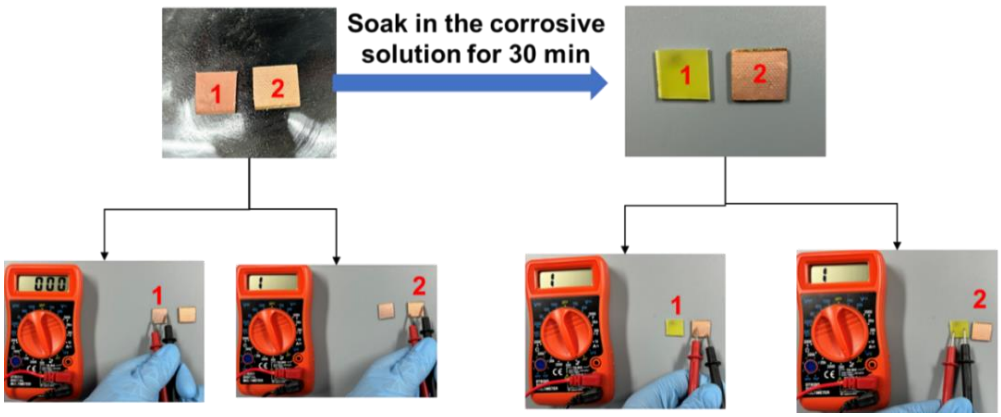

Fig. S21. Component 1 and 2 are the traditional copper-clad plates (CCL), of these, CCL2 is coated by EP-FCB. After soaking in the corrosive solution for 30 min, the copper on CCL1 is corroded, while CCL2 is intact. This proves that the prepared resin has a protective effect on the components.

- **Healability of EP-CB for mechanical damage:**

Compared to EP-FCB, only under the condition of 180°C/3MPa for 30 min, the fractured EP-CB samples can be rejoined completely (Fig. S19), and the healed EP-CB has mechanical strength (Fig. S20). However, the healing efficiency based on tensile strain is only 4%. These results further indicate that epoxy with fluorine-substituted

carbamate bonds has better healability for mechanical damage.

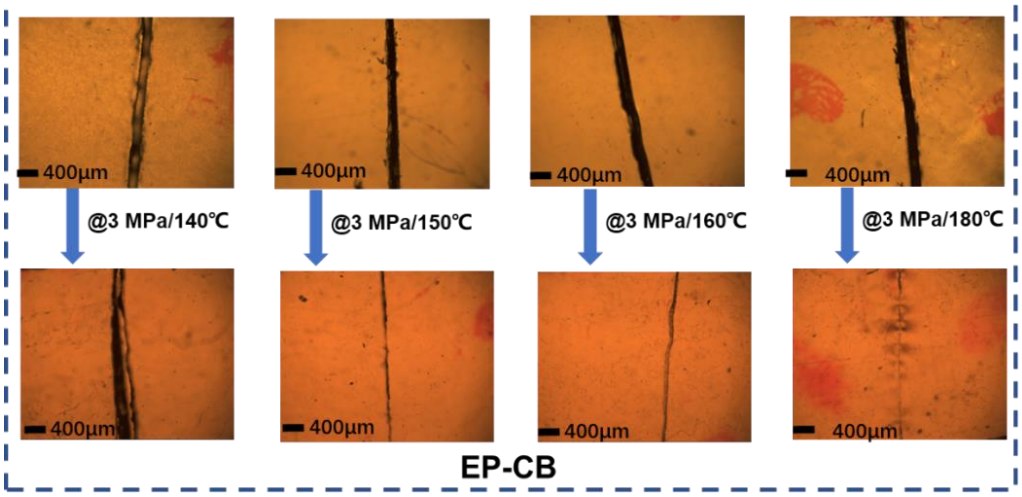

Fig. S22. Optical micrographs of EP-CB samples before and after healing under different temperatures.

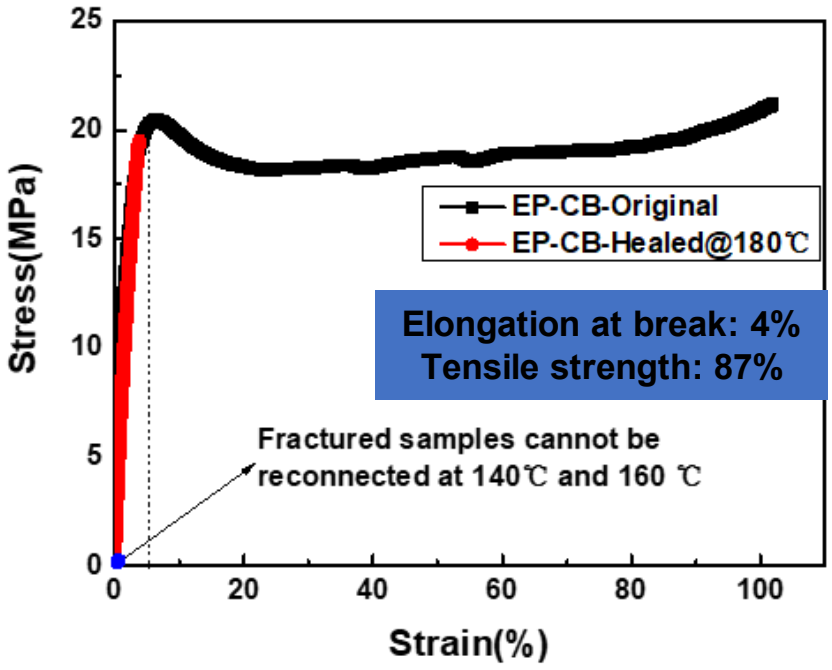

Fig. S23. Stress-strain curves for the original and healed EP-CB samples under different healing temperature.

Table S5. Comparison the mechanical strength of EP-FCB with recently reported dynamic bonds-crosslinking epoxy resins.

References	Dynamic structures	Mechanical strength (MPa)	Elastic modulus (MPa)
[2]	Hindered urea bond	22.6	440
[3]	Dynamic ester bond	16.62	-
[4]	Dynamic disulfide bond	33	-
[5]	Dynamic disulfide bond	11.7	6.81
[6]	Dynamic diacetal motif	13	244
[7]	Dynamic imine bond	7.7	41.4
[8]	Dynamic ester bond	25	-
[9]	Dynamic disulfide bond	24	860
This work	**Dynamic fluorine-substituted carbamate bond**	**33.4**	**1217**

References

[1] W. Y. Zhou and J. Zuo, J. Reinf. Plast. Compos., 2013, 32, 1359–1369.

[2] W.J. Sun, L. Zhang, Y.J. Liang, J.Z. Xu, Y. Gao, J.M. Luo and Y.H. Cheng, React. Funct. Polym., 2022, 176, 105307.

[3] X.X. Yang, L.Z. Guo, X. Xu, S.B. Shang and H. Liu, Mater. Des., 2020, 185, 108248.

[4] H. Memon and Y. Wei, J. Appl. Polym. Sci., 2020, 137, e49541.

[5] S.J. Shan, D.D. Mai, Y.L. Lin and A.Q. Zhang, ACS Appl. Polym. Mater., 2021, 3, 5115-5124.

[6] W.X. Zhang, F. Gao, X.J. Chen, L. Shen, Y.J. Chen and Y.J. Lin, ACS Sustainable Chem. Eng., 2023, 3065-3073.

[7] Y.Y. Liu, J. He, Y.D. Li, X.L. Zhao, and J.B. Zeng, Compos. Commun., 2020, 22, 100445.

[8] T. Liu, C. Hao, L.W. Wang, Y.Z. Li, W.C. Liu, J.N. Xin and J.W. Zhang, Macromolecules, 2017, 50, 8588-8597.

[9] A. Takahashi, T. Ohishi, R. Goseki and H. Otsuka, Polymer, 2016, 82, 319-326.